Journal of Marine Science and Technology

Volume 23 | Issue 5 Article 3

ANALYSIS OF THE DYNAMICS OF A FLOATING BODY WITH THIN SKIRTS BY USING THE DUAL BOUNDARY ELEMENT METHOD

Wen-Kai Weng
Research Center for Ocean Energy and Strategies, National Taiwan Ocean University, Keelung, Taiwan, R.O.C.,
wkweng@mail.ntou.edu.tw

Ruey-Syan Shih
Department of Construction and Spatial Design, Tungnan University, New Taipei City, Taiwan, R.O.C.

Duc-Tru Tran
Research Center for Ocean Energy and Strategies, National Taiwan Ocean University, Keelung, Taiwan, R.O.C.

Recommended Citation

Weng, Wen-Kai; Shih, Ruey-Syan; and Tran, Duc-Tru (2015) "ANALYSIS OF THE DYNAMICS OF A FLOATING BODY WITH THIN SKIRTS BY USING THE DUAL BOUNDARY ELEMENT METHOD," *Journal of Marine Science and Technology*: Vol. 23: Iss. 5, Article 3.
DOI: 10.6119/JMST-015-0205-2
Available at: https://jmstt.ntou.edu.tw/journal/vol23/iss5/3

Journal of Marine Science and Technology, Vol. 23, No. 5, pp. 598-607 (2015)
DOI: 10.6119/JMST-015-0205-2

ANALYSIS OF THE DYNAMICS OF A FLOATING BODY WITH THIN SKIRTS BY USING THE DUAL BOUNDARY ELEMENT METHOD

Wen-Kai Weng[1], Ruey-Syan Shih[2], and Duc-Tru Tran[1]

Key words: moored floating structure, rigid skirts, numerical simulation, drag coefficient, dual boundary element method.

ABSTRACT

In this study, a numerical simulation of the dynamic behavior of a novel floating structure with rigid skirts was conducted using the dual boundary element method. The thickness of the skirts mounted beneath the structure was negligible. A theoretical analysis was derived from linear wave theory, and a nonlinear drag term was added in the motion equation of the floating structure for improving the solution.

This study investigated the effects of double vertical skirts on a free floating structure and verified the validity of the analysis by comparing the result with those of Gesraha (2006). The results showed that adding double vertical skirts increases the overall mass of the structure, thus enabling the floating structure to resist wave forces for longer periods.

The main purpose of this paper was to investigate the influences of the angles of the skirt attachment and the nonlinear drag term, on the moored floating structure. This study focused on the changes in the structure's motion in each mode, reflection and transmission coefficients, energy loss induced by the nonlinear drag term, and various angles of skirt attachment. The analytical results agreed with the experimental data. Involving a nonlinear drag term in the analysis yielded superior results, particularly when the structure approached the natural period in the three modes of oscillation.

I. INTRODUCTION

Floating structures are increasingly used in the near shore regions for absorbing wave energy and prevent shoreline erosion. In addition, Floating structures are inexpensive and can be easily installed. They can also be designed to meet specific aesthetic and functional requirements. However, despite their universal advantages, floating structure are used mostly in low-wave-energy regions.

In recent years, Sannasiraj et al. (1998, 2000) utilized the two-dimensional finite element method to analyze the mooring forces and the responses of a single floating pontoon-type breakwater; this method has also been adopted to evaluate the hydrodynamic coefficients and the responses in the sway and heave of multiple floating structures. Gesraha (2006) studied the reflection and transmission of incident waves interacting with a long rectangular breakwater with two thin sideboards protruding vertically downward in the form of eigenfunction expansions. The exciting forces, added-mass and damping coefficients, responses of the structure, and the transmission coefficient were also examined. Lee and Cho (2003) numerically evaluated how an incident wave interacted with a moored pontoon-type floating breakwater. In addition, several researches have focused on developing various forms of floating structures and investigating their efficiencies. McCartney (1985) classified floating breakwaters into four categories and discussed the advantages and disadvantages of various structures, mooring systems, and anchorage methods. Isaacson et al. (1998) compiled the responses of a floating breakwater and compared the results with experimental and field data. Murali et al. (1997) experimentally investigated the reflection and transmission characteristics of cage-floating breakwaters. Wang (2010) experimentally studied a floating breakwater fabricated using several diamond-shaped blocks. Besides, Lee and Ker (2002) used an analytical solution to solve the surge motion of tension leg platform and problem of linear waves with a porous tension leg platform. Discussion also included drag forces on mooring cables. Williams (1996) investigated the behavior of a submerged breakwater of rectangular cross section, The viscous-dissipation coefficients were applied in the motion equation of structure. It assumed that viscous effects can be modeled using independent flow fields formulation and that these effects do not contribute significantly to the exciting loads on the structure. Huang and Tang (2009) studied the wave-body interaction of floating dual pontoon structures in a two-dimension fully nonlinear numerical wave tank based on

Paper submitted 02/17/14; revised 01/08/15; accepted 02/05/15. Author for correspondence: Wen-Kai Weng (e-mail: wkweng@mail.ntou.edu.tw).
[1] Research Center for Ocean Energy and Strategies, National Taiwan Ocean University, Keelung, Taiwan, R.O.C.
[2] Department of Construction and Spatial Design, Tungnan University, New Taipei City, Taiwan, R.O.C.

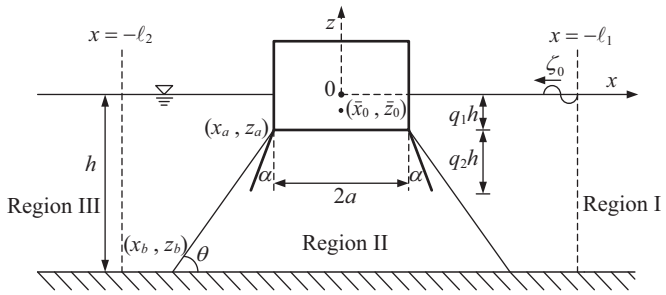

Fig. 1. Definition sketch.

the boundary integral equation method. Lu (2011) presents two-dimensional numerical results of the dependence of wave forces of multiple floating bodies in close proximity on the incident wave frequency, gap width, body draft, body breadth and body number based on both viscous fluid and potential flow model.

In this study, a numerical model was developed for analyzing the behaviors of a floating structure by using the dual boundary element method (DBEM). The response amplitude operators, reflection and transmission coefficients, and energy loss induced by the drag effect were calculated and analyzed for different angles of skirt attachment with the whole range of a dimensionless parameter *ka*.

II. THEORETICAL FORMULAE

As Fig. 1 shows, a moored floating structure of a rectangular cross-section, with width $2a$ and draft q_1h, and with thin, rigid plates attached to its bottom, was on a sea of uniform depth h. The thickness of the plates was negligible compared with the depth of the water and was adopted as zero. Cartesian coordinates were employed with the z-axis directed vertically upwards from its origin on the undisturbed free surface. The structure was located symmetrically at $x = 0$ and linked to the sea floor by using an idealized mooring system. The motions of the structure, when subjected to a train of small amplitude waves of a height of $2\zeta_0$ and frequency σ traveling in the negative x-direction, were assumed to be small and linear. The fluid in the interesting region was assumed to be inviscid and incompressible. In addition, the motion of the fluid was irrotational and can be described in terms of velocity potential $\Phi(x, z; t) = g\zeta_0/\sigma.\phi(x, z)e^{i\sigma t}$. The potential of the analytical region conformed to Laplace's equation.

$$\nabla^2\phi(x,z) = 0 \tag{1}$$

The analytical region was divided into three sub-regions by applying of two auxiliary boundaries ($x = l_1, -l_2$) for analyzing the problem. The sub-regions were termed as Region (I), (II), and (III), and were denoted by their complex potentials as $\phi_j (j = 1, 2, 3)$. If the auxiliary boundaries are set far enough from the structure for wave motions in Regions (I) and (III) to be unaffected by the evanescent waves induced by the structure, then the potentials of Region (I) and (III) can be described as follows:

$$\phi_1(x,z) = \left[e^{ik(x-l_1)} + K_r e^{-ik(x-l_1)} \right] \frac{\cosh k(h+z)}{\cosh kh} \tag{2}$$

$$\phi_3(x,z) = K_t e^{ik(x+l_2)} \frac{\cosh k(h+z)}{\cosh kh} \tag{3}$$

In complex forms, K_r and K_t are reflection and transmission coefficients, respectively. k is the incident wave number, which is the root of the linear dispersion relationship $\sigma^2 = gk \tanh kh$. The potentials of Region (I) and (III), combined with their normal derivatives at auxiliary boundaries $x = \ell_1$ and $x = -\ell_2$, are expressed as:

$$\phi_1(\ell_1,z) = (1+K_r)\frac{\cosh k(h+z)}{\cosh kh} \tag{4}$$

$$\bar{\phi}_1(\ell_1,z) = ik(1-K_r)\frac{\cosh k(h+z)}{\cosh kh} \tag{5}$$

$$\phi_3(-\ell_2,z) = K_t \frac{\cosh k(h+z)}{\cosh kh} \tag{6}$$

$$\bar{\phi}_3(-\ell_2,z) = -ikK_t \frac{\cosh k(h+z)}{\cosh kh} \tag{7}$$

Region (II) is enclosed by the free surface S_f, the immersed structure surface S_b, the impermeable sea-floor surface S_s, and two fictitious boundaries S_1, S_2. The boundary conditions on the free surface and sea floor are subject to the following equations, respectively:

$$\frac{\partial\phi_2}{\partial z} = \frac{\sigma^2}{g}\phi_2 \quad \text{when } z = 0 \tag{8}$$

$$\frac{\partial\phi_2}{\partial z} = 0 \qquad \text{when } z = -h \tag{9}$$

The requirements of continuity of mass and energy flux across the fluid interfaces between each region imply the following matching conditions:

$$\phi_1 = \phi_2 \qquad \text{when } x = \ell_1 \tag{10}$$

$$\frac{\partial\phi_1}{\partial x} = \frac{\partial\phi_2}{\partial x} \qquad \text{when } x = \ell_1 \tag{11}$$

$$\phi_2 = \phi_3 \qquad \text{when } x = -\ell_2 \tag{12}$$

$$\frac{\partial\phi_2}{\partial x} = \frac{\partial\phi_3}{\partial x} \qquad \text{when } x = -\ell_2 \tag{13}$$

The floating structure is assumed to be homogenous and shows a small amplitude of surge, heave and pitch motions in response to the incident and diffracted waves. The displacement for the three modes of motion may be expressed as:

$$\hat{X} = x_0 - \overline{x}_0 = \xi e^{i\sigma t}, \hat{Z} = z_0 - \overline{z}_0 = \eta e^{i\sigma t}, \hat{\delta} = \omega e^{i\sigma t} \quad (14)$$

where, $(\overline{x}_o, \overline{z}_o)$ is the coordinate of the center of mass of the structure at rest; and (x_o, z_o) is its instantaneous position. ξ, η and ω are amplitudes of surge, heave, and pitch motions, respectively. When the floating structure is subjected to wave motion, the first order kinematic boundary on the immersed surface of the structure may be written as:

$$\frac{\partial \Phi_b}{\partial n} = \frac{\partial \hat{X}}{\partial t}\frac{\partial x}{\partial n} + \frac{\partial \hat{Z}}{\partial t}\frac{\partial z}{\partial n} + \frac{\partial \hat{\delta}}{\partial t}\left[\frac{\partial x}{\partial n}(z - \overline{z}_o) - \frac{\partial z}{\partial n}(x - \overline{x}_o)\right] \quad (15)$$

The equation of the structure's motion under the effect of the hydrodynamic wave forces, restoring force, mooring forces and viscous drag may be expressed as:

$$m\ddot{\hat{X}} + F_{kx} + F_{dx} = \int_{S_b} p\frac{\partial x}{\partial n}ds \quad (16a)$$

$$m\ddot{\hat{Z}} + F_{kz} + F_{dz} + F_r = \int_{S_b} p\frac{\partial z}{\partial n}ds \quad (16b)$$

$$I_o\ddot{\hat{\delta}} + M_{k\delta} + M_{dm} + M_r = \int_{S_b} p[(z - \overline{z}_o)\frac{\partial x}{\partial n} - (x - \overline{x}_o)\frac{\partial z}{\partial n}]ds \quad (16c)$$

where, m is the mass of the structure, I_0 is the mass moment of inertia around the center of the mass of the structure, p is the dynamic pressure of the fluid, and F_r, and M_r are the restoring force and moment, respectively. The foregoing pressure of the fluid and restoring components are denoted by

$$p = -i\rho g\varsigma_o\phi \cdot e^{i\sigma t} \quad (17a)$$

$$F_r = \rho g\hat{Z}\int_{S_b}\frac{\partial z}{\partial n}ds \quad (17b)$$

$$M_r = \rho g\hat{\delta}\int_{S_b}(x - \overline{x}_o)[(z - \overline{z}_o)\frac{\partial x}{\partial n} - (x - \overline{x}_o)\frac{\partial z}{\partial n}]ds \quad (17c)$$

The mooring system is considered the symmetric fore and aft of the structure. Considering a mooring line AB, with its spring constant K and pretension F_o, the coordinates of the attachment point on the structure and sea floor are (x_a, z_a) and (x_b, z_b), respectively. By disregarding the inertia effects of the mooring line and the viscous forces on the line, Weng (2007) derived each component of the forces and moments by using the mooring system:

$$F_{kx} = K_{xx}\hat{X} + K_{\delta x}\hat{\delta} \quad (18a)$$

$$F_{kz} = K_{zz}\hat{Z} \quad (18b)$$

$$M_{k\delta} = K_{x\delta}\hat{X} + K_{\delta\delta}\hat{\delta} \quad (18c)$$

where

$$K_{xx} = 2[\frac{(x_b - x_a)^2}{l_{ab}^2}K + \frac{(z_b - z_a)^2}{l_{ab}^2}\frac{F_0}{l_{ab}}]$$

$$K_{zz} = 2[\frac{(z_b - z_a)^2}{l_{ab}^2}K + \frac{(x_b - x_a)^2}{l_{ab}^2}\frac{F_0}{l_{ab}}]$$

$$K_{x\delta} = K_{\delta x} = 2\left\{\frac{(x_b - x_a)}{l_{ab}^2}\left[(x_b - x_a)(z_a - \overline{z}_0) - (z_b - z_a)(x_a - \overline{x}_0)\right]K + \frac{(z_b - z_a)}{l_{ab}^2}\left[(z_b - z_a)(z_a - \overline{z}_0) + (x_b - x_a)(z_a - \overline{z}_0)\right]\frac{F_0}{l_{ab}}\right\}$$

$$K_{\delta\delta} = 2\frac{1}{l_{ab}^2}\left\{\left[(x_b - x_a)(z_a - \overline{z}_b) - (z_b - z_a)(x_a - \overline{x}_0)\right]^2 K + \left[(z_b - z_a)(z_a - \overline{z}_b) + (x_b - x_a)(x_a - \overline{x}_0)\right]^2\frac{F_0}{l_{ab}}\right\}$$

The drag force due to the water-particle velocity is negligible when compared with the structural velocity. Chakrabarti (1983) computed the drag force and moment in a particular direction and expressed it in terms of a drag coefficient times the structural velocity squared team:

$$F_{dx} = \frac{1}{2}\rho C_{dx}\dot{\hat{X}} \mid \dot{\hat{X}} \mid (q_1 h + q_2 h\cos\alpha) \quad (19a)$$

$$F_{dz} = \frac{1}{2}\rho C_{dz}\dot{\hat{Z}} \mid \dot{\hat{Z}} \mid 2(a + q_2 h\sin\alpha) \quad (19b)$$

$$M_{dm} = \frac{1}{2}\rho C_{dm}\left[\int_0^{a+q_2 h\sin\alpha} 2r\dot{\hat{\delta}}\int \mid r\dot{\hat{\delta}} \mid rdr + \int_0^{-q_1 h - q_2 h\cos\alpha} r\dot{\hat{\delta}}\int \mid r\dot{\hat{\delta}} \mid rdr\right] \quad (19c)$$

where, C_{dx}, C_{dz}, C_{dm} are the drag force coefficients of surge, heave, and pitch motions of the floating structure, respectively. The nonlinear drag terms were linearized by expanding in a Fourier series and retaining only the first term. These terms were written in a linear form as:

$$F_{dx} = \frac{4i}{3\pi}\rho C_{dx}\sigma^2\xi\,|\,\xi\,|\,(q_1 h + q_2 h\cos\alpha)e^{i\sigma t} \tag{20a}$$

$$F_{dz} = \frac{4i}{3\pi}\rho C_{dz}\sigma^2\eta\,|\,\eta\,|\,2(a + q_2 h\sin\alpha)e^{i\sigma t} \tag{20b}$$

$$M_{dm} = \frac{4i}{3\pi}\rho C_{dm}\sigma^2\omega\,|\,\omega\,|\,[\frac{(a+q_2 h\sin\alpha)^4}{2} + \frac{(q_1 h + q_2 h\cos\alpha)^4}{2}]e^{i\sigma t} \tag{20c}$$

III. DEVELOPMENT OF THE THEORY

1. Coefficients of Reflection and Transmission

The coefficients of reflection and transmission are determined using the continuity of mass and energy flux on the fictitious boundaries. Substituting Eq. (5) into Eq. (11), multiplying with $\cosh k(h+z)$, and integrating from $z = -h$ to $z = 0$, the reflection coefficient, K_r, can be expressed in terms of the normal derivatives of potential, $\bar{\phi}_1$, as:

$$K_r = 1 + \frac{i}{N_0 \sinh kh}\int_{-h}^{0}\bar{\phi}_1\cosh k(h+z)dz \quad \text{on } x = \ell_1 \tag{21}$$

where $N_0 = \left[1 + 2kh/\sinh 2kh\right]/2$.

Substituting Eq. (21) into Eq. (4), associating with Eq. (10), the relationship between the potential of the auxiliary boundary, $x = \ell_1$, and its normal derivative can be written as:

$$\phi(\ell_1, z) = 2\frac{\cosh k(h+z)}{\cosh kh} + 2i\frac{\cosh k(h+z)}{N_0 \sinh 2kh}\int_{S_1}\bar{\phi}(\ell_1, z)\cosh k(h+z)ds \tag{22}$$

Similarly, the coefficient of transmission can be derived by substituting Eq. (7) into Eq. (13), multiplying with $\cosh k(h+z)$, and integrating from $z = -h$ to $z = 0$, to yield the following form:

$$K_t = \frac{i}{N_0 \sinh kh}\int_{-h}^{0}\bar{\phi}_2\cosh k(h+z)dz \quad \text{on } x = -\ell_2 \tag{23}$$

The relationship between the potential and its normal derivative on the auxiliary boundary, $x = -\ell_2$, can be obtained by substituting Eq (23) into Eq. (6), and associating with Eq. (12):

$$\phi(-\ell_2, z) = 2i\frac{\cosh k(h+z)}{N_0 \sinh 2kh}\int_{-h}^{0}\bar{\phi}(-\ell_2, z)\cosh k(h+z)ds \tag{24}$$

2. Motion of Floating Structure

The motion amplitude of the structure is determined by stating Eq. (16), in terms of the potential ϕ_b on the immersed surface of structure, as follows:

$$\xi/\varsigma_o = \frac{i}{\lambda_4}\left\{\lambda_3\cdot\int_{S_b}\phi_b\frac{\partial x}{\partial n}ds + \lambda_2\cdot\int_{S_b}\phi_b[(z-\bar{z}_o)\frac{\partial x}{\partial n} - (x-\bar{x}_o)\frac{\partial z}{\partial n}]ds\right\} \tag{25}$$

$$\eta/\varsigma_o = \frac{i}{\beta}\int_{S_b}\phi_b\frac{\partial z}{\partial n}ds \tag{26}$$

$$\omega/\varsigma_o = \frac{i}{\lambda_4}\left\{\lambda_2\cdot\int_{S_b}\phi_b\frac{\partial x}{\partial n}ds + \lambda_1\cdot\int_{S_b}\phi_b[(z-\bar{z}_o)\frac{\partial x}{\partial n} - (x-\bar{x}_o)\frac{\partial z}{\partial n}]ds\right\} \tag{27}$$

where

$$\lambda_1 = \frac{m}{\rho}\cdot\frac{\sigma^2}{g} - \frac{K_{xx}}{\rho g} - \frac{4i}{3\pi}C_{dx}\frac{\sigma^2}{g}\left|\xi\right|(q_1 h + q_2 h\cos\alpha)$$

$$\lambda_2 = \frac{K_{x\delta}}{\rho g}$$

$$\lambda_3 = \frac{I_o}{\rho}\cdot\frac{\sigma^2}{g} - \frac{K_{\delta\delta}}{\rho g} - \int_{S_b}(x-\bar{x}_o)[(z-\bar{z}_o)\frac{\partial x}{\partial n} - (x-\bar{x}_o)\frac{\partial z}{\partial n}]ds - \frac{2i}{3\pi}C_{dm}\frac{\sigma^2}{g}\left|\omega\right|[(a+q_2 h\sin\alpha)^4 + (q_1 h + q_2 h\cos\alpha)^4]$$

$$\lambda_4 = \lambda_1\lambda_3 - \lambda_2^2$$

$$\beta = \frac{m}{\rho}\cdot\frac{\sigma^2}{g} - \frac{K_{zz}}{\rho g} - \int_{S_b}\frac{\partial z}{\partial n}ds - \frac{8i}{3\pi}C_{dx}\frac{\sigma^2}{g}\left|\eta\right|(a + q_2 h\sin\alpha)$$

Eqs. (25)~(27) are the amplitudes of surge, heave, and pitch motions of the structure, respectively. Substituting Eqs. (25)~(27) into Eq. (15), and associating with Eq. (14), the potential on the immersed surface of the structure can be written as:

$$\frac{\partial\phi}{\partial n} = -\frac{\sigma^2}{g}\left\{\frac{\lambda_2}{\lambda_4}\frac{\partial x}{\partial n} + \frac{\lambda_1}{\lambda_4}[(z-\bar{z}_o)\frac{\partial x}{\partial n} - (x-\bar{x}_o)\frac{\partial z}{\partial n}]\right\}\cdot\int_{S_b}\phi[(z-\bar{z}_o)\frac{\partial x}{\partial n} - (x-\bar{x}_o)\frac{\partial z}{\partial n}]ds - \frac{\sigma^2}{g}\left\{\frac{\lambda_3}{\lambda_4}\frac{\partial x}{\partial n} + \frac{\lambda_2}{\lambda_4}[(z-\bar{z}_o)\frac{\partial x}{\partial n} - (x-\bar{x}_o)\frac{\partial z}{\partial n}]\right\}\cdot\int_{S_b}\phi\frac{\partial x}{\partial n}ds - \frac{\sigma^2}{g}\frac{1}{\beta}\cdot\int_{S_b}\phi\frac{\partial z}{\partial n}ds \tag{28}$$

3. Dual Boundary Element Method

The above problem for the fluid potential of Region (II) is solved numerically by using the DBEM. According to Green's second identity law, the first equation of the DBEM for the potential of any point on the boundaries of Region (II) is subject to the potential on the boundaries combined with its first normal derivative.

$$\pi\phi(\xi',\eta') = \int_{\Gamma_2} [\frac{\partial\phi(\xi,\eta)}{\partial n_{xz}}(\ln\frac{1}{r}) - \phi(\xi,\eta)\frac{\partial}{\partial n_{xz}}(\ln\frac{1}{r})ds \qquad (29)$$

where, $\ln 1/r$ is the solution of Laplace equation. n_{xz} is the normal vector of point (ξ, η). When the boundaries enclosing Region (II) are partitioned into N segments, Eq. (29) indicates a matrix form as follows:

$$\left[G_{ij}\right]\{\phi_i\} = \left[H_{ij}\right]\left\{\frac{\partial\phi}{\partial n_j}\right\} \quad (i,j=1,2,...,N) \qquad (30)$$

The second equation of the dual boundary integral formulation for the points on the boundaries is derived as:

$$\pi\frac{\partial\phi(\xi',\eta')}{\partial n_{\overline{xz}}} = \int_{\Gamma_2} [\frac{\partial\phi(\xi,\eta)}{\partial n_{xz}}\frac{\partial}{\partial n_{\overline{xz}}}(\ln\frac{1}{r}) - \phi(\xi,\eta)\frac{\partial^2}{\partial n_{xz}\partial n_{\overline{xz}}}(\ln\frac{1}{r})]ds \qquad (31)$$

where, $n_{\overline{xz}}$ is the normal vector of point (ξ', η'). Eq. (31) also displays a matrix form:

$$\left[\overline{G}_{ij}\right]\{\phi_i\} = \left[\overline{H}_{ij}\right]\left\{\frac{\partial\phi}{\partial n_j}\right\} \quad (i,j=1,2,...,N) \qquad (32)$$

Matrices of Eqs. (30) and (32) are dependent on the geography of the analytical domain and have been derived by Chen (1983). Boundaries of the rigid skirts of the floating structure are degenerate boundaries since the thicknesses of the rigid skirts is assumed to be zero. Eqs. (30) and (32) are a linearly dependent equations and cannot be solved directly. However, the degenerated system can be desingularized by rearranging the matrix of degenerate boundaries between Eqs. (30) and (32), and formulating a new independent equations as follows:

$$\left[G^*_{ij}\right]\{\phi_i\} = \left[H^*_{ij}\right]\left\{\frac{\partial\phi}{\partial n_j}\right\} \quad (i,j=1,2,...,N) \qquad (33)$$

Substituting the boundary conditions of Region II, and Eqs. (8), (9), (22), (24), and (28), into Eq. (33), the potential and its normal derivative on the boundaries of Region II can be obtained. The motion amplitude of each mode and the coefficients of reflection and transmission can also be acquired by substituting the potential on the immersed surface of the structure into Eqs. (25)~(27) and Eqs. (21) and (23).

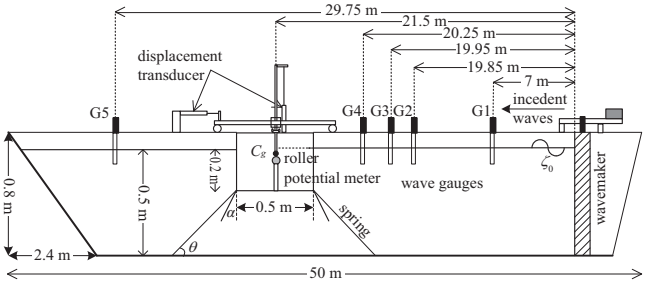

Fig. 2. The experimental setup in detail.

IV. EXPERIMENTAL SETUP

A series of experiments were conducted in a two dimensional piston-type wave flume for verifying numerical results. The flume was 50 m long, 1.0 m wide, and 0.8 m high. An artificial beach with a slope of approximately 1:3 and covering a horizontal distance of 2.4 m was installed at the end of damping zone of the wave flume.

A floating structural model, 50 cm long, 96 cm wide, and 20 cm high, was set at a distance of approximately 21.5 m from the wave maker paddle for the experiment. The model was equipped with two skirts, both 15 cm long and 0.2 cm thick, and consisted of acrylic fiber at the fore and aft. The mass and mass moment of inertia of the floating structural model were approximately 43 kg and 1.16 kg.m^2, respectively. The position of the model's center of mass was 10 cm under the free surface. Four taut springs, each with a spring stiffness K of 0.085 kgf/cm in air, pretension force of 1.44 kgf, and an incline of 60^0 to the horizontal bottom, were employed to anchor the test model.

Five wave gauges were set up for recording the wave evolution. The gauges G1 and G5 were for the incident and transmitted waves, respectively, and G2, G3, and G4 were for the reflected waves. Moreover, two position transducers and a roller potentiometer were also mounted on the model for measuring the displacement and rotating angle of the model. The detailed setup is shown in Fig. 2.

The three-mode displacements of the floating structure and its reflection coefficients were investigated during the model test. In this paper, the reflection coefficients were obtained by the analytical method of Goda and Suzuki (1976).

The model test was performed with regular waves, and the wave conditions for linear waves were selected from 0.8 to 2.5 s for the wave period and 5 to 7 cm for the wave height. The water depth was maintained at a constant of 0.5 m throughout all model tests.

V. RESULTS AND DISCUSSIONS

1. Verification of Numerical Model in Free Body with Vertical Skirts

The efficiency of the numerical model in simulating free body dynamics with or without rigid skirts was verified by

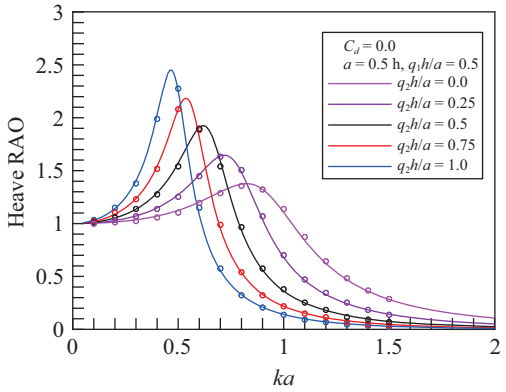

Fig. 3. Comparison between simulated and Gesraha results heave RAO with a = 0.5h, q_1h/a = 0.5 and α = 0°. (Line: present results; dot: Gesraha results)

comparing the results with the results of Gesraha (2006). As shown in Fig. 3, a good agreement between the present analysis (line) and the results of the eigenfunction expansion method (dot) derived by Gesraha can be clearly observed over the whole analytical range. Obviously, the duration of the peak of the structure's heave motion tends to increase with the length of the skirts. This increase suggests that a change in the natural frequency of the structure's heave motion occurs because of the skirts. The purpose of making changes in the natural frequency of the structure's motion was that water under the inner skirts follows the floating structure's movement, and this gave an additional mass to the structure when it was in motion.

2. Motion of Moored Floating Structure with Skirts

The response amplitude operators in surge, heave and pitch of the moored floating structure as a function of the dimensionless parameter ka were analyzed for various angles of skirts attachments (α = 0°, 30°, 60°, 90°). The numerical analysis proceeded per the conditions of experimental installation, and the drag coefficient in each mode of motion was assumed to be of the same value for simplifying the problem, i.e, $C_d = C_{dx} = C_{dz} = C_{dm}$. The results of the analysis are presented in Figs. 4~7.

Figs. 4~7 illustrate the numerical and experimental amplitudes of the three-mode motions of the structure with vertical (α = 0°) or inclined (α = 30°, 60°, 90°) skirts, modulating the dimensionless parameter ka. Different drag coefficients (C_d = 0.0, 1.0, 2.0, 3.0) were applied to understand the effects of drag force on the structure's motions in the numerical analysis. Solutions were obtained in an iterating manner. The amplitude in each mode of the structure's motion was initially assumed to be zero, and a new set of values of motion amplitude were obtained using Eq. (33) for the next iteration. The process was repeated until a numerical convergence was achieved in the amplitudes of each mode of the structure's motion.

The numerical solution for the results cited in Figs. 4~7 is shown as a solid line. While the scattering of the experimental

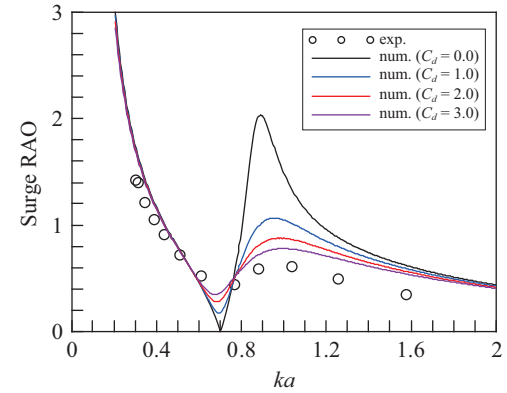

(a) Surge of moored floating structure with skirts.

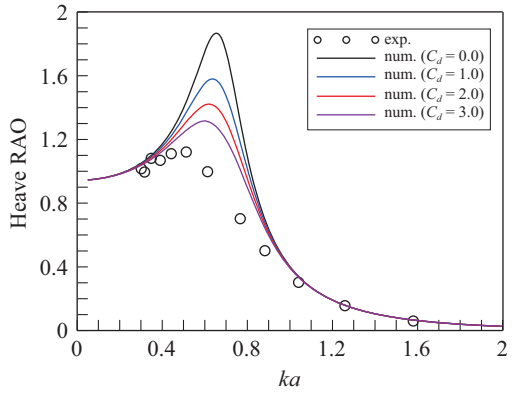

(b) Heave of moored floating structure with skirts.

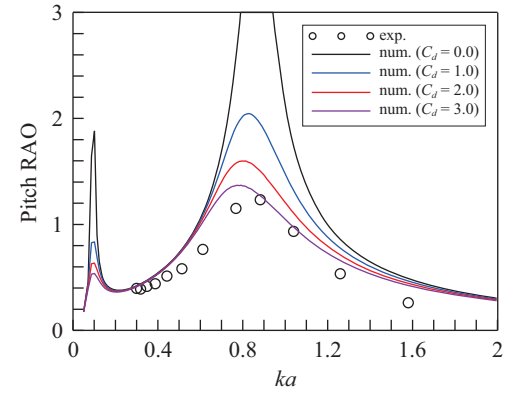

(c) Pitch of moored floating structure with skirts.

Fig. 4. Correlation of three modes motion of moored floating structure with skirts (a = 0.5 h, q_1 = 0.4 and α = 0°).

data may be because of differing amounts of nonlinear damping with different wave heights, the correlation between numerical and experimental results is much better with this added nonlinear damping term. The nonlinear damping term provides a better solution particularly when the structure is approaching its natural period in three modes of oscillation. As illustrated in the figures, the oscillation values of the analytical results around the natural period of the structure gradually decrease and approach the experimental results as the drag coefficient increases from 0.0 to 3.0.

Figs. 4~7 show that, as the skirts attached to the bottom of

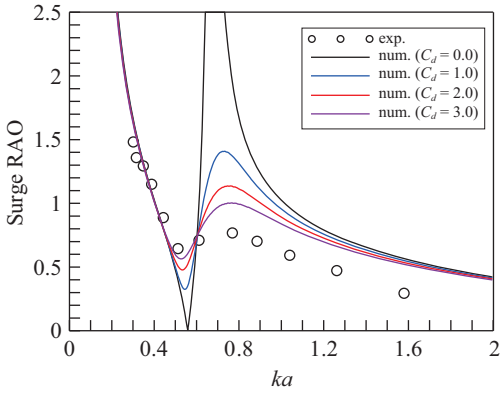

(a) Surge of moored floating structure with skirts.

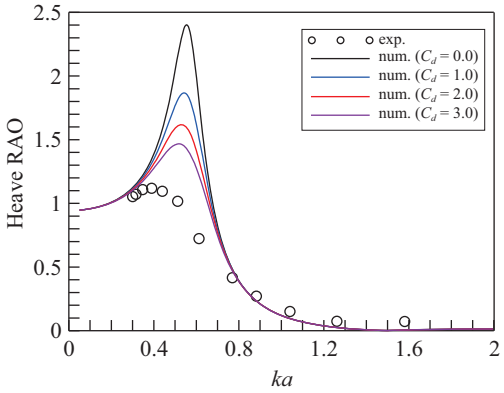

(b) Heave of moored floating structure with skirts.

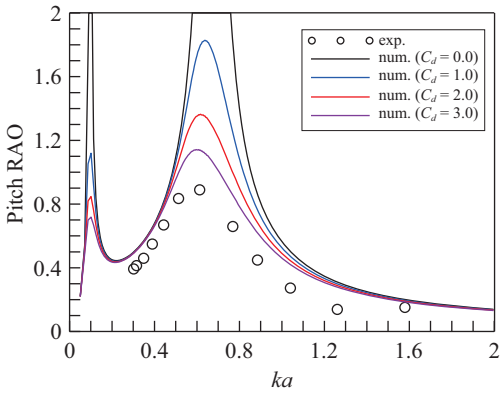

(c) Pitch of moored floating structure with skirts.

Fig. 5. Correlation of three modes motion of moored floating structure with skirts (a = 0.5h, q_1 = 0.4 and α = 30°).

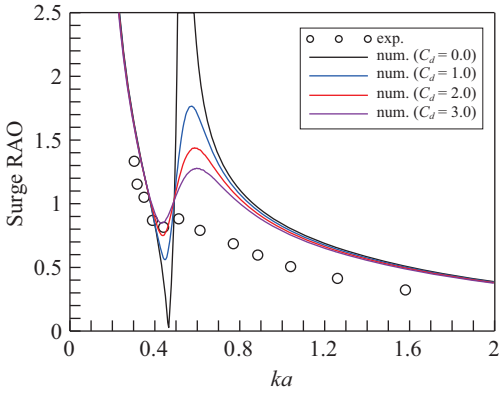

(a) Surge of moored floating structure with skirts.

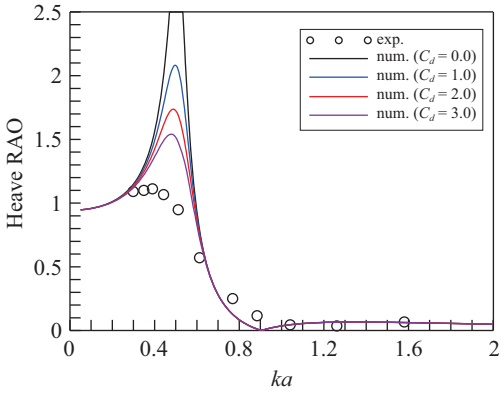

(b) Heave of moored floating structure with skirts.

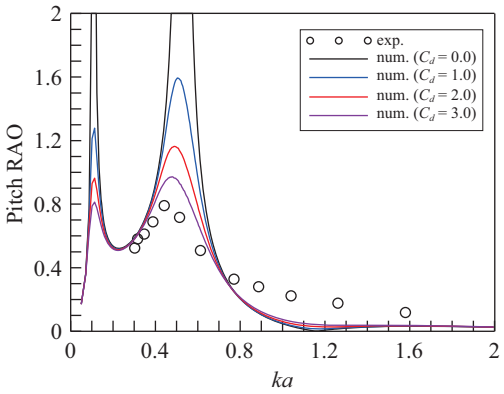

(c) Pitch of moored floating structure with skirts.

Fig. 6. Correlation of three modes motion of moored floating structure with skirts (a = 0.5h, q_1 = 0.4 and α = 60°).

the structure gradually increased their angles of attachment from 0° to 90°, the natural period of the structure in each mode of oscillation increased. Moreover, the oscillation of the structure in each mode decreased in range as the natural period approached when the skirts were horizontally directed. This indicated that extending the angle of the skirts increased its overall mass when it was in motion.

3. Reflection and Transmission Coefficients and Energy Loss

In general, a floating structure provides effective defense against wave energy in low-tide area. However, the natural period of the structure in each oscillation mode has a profound effect on wave reflection and the transmission coefficient. Figs. 8(a)~(d) shows the correlation between the reflection coefficient and ka when the angles of skirt attachment were α = 0°, 30°, 60°, 90°. Except for the case of the structure with vertical skirts (Fig. 8(a), α = 0°), the experimental reflection coefficients increased nearly linearly when the incoming wave period decreased. Furthermore, the experimental results displayed no significant difference when the skirts were set up in an oblique angle (α = 30°, 60°, and 90°). In the test case of the

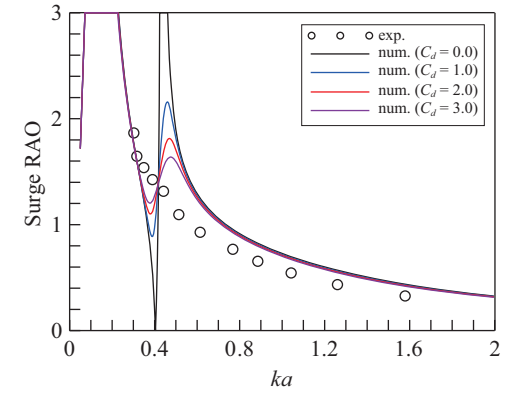

(a) Surge of moored floating structure with skirts.

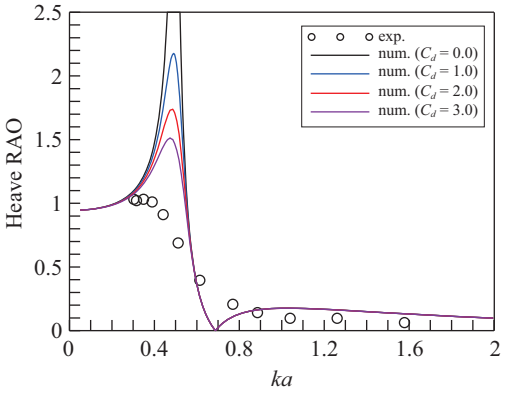

(b) Heave of moored floating structure with skirts.

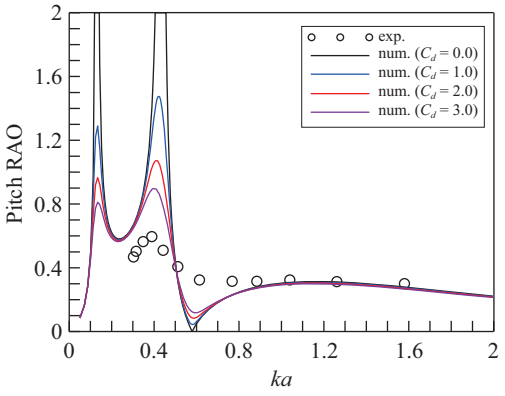

(c) Pitch of moored floating structure with skirts.

Fig. 7. Correlation of three modes motion of moored floating structure with skirts (a = 0.5h, q_1 = 0.4 and α = 90°).

structure with vertical skirts, the reflection coefficient varied significantly as the natural period of the structure approached. The result of each analytical case is shown in Figs. 7(a)~(d) and represented as a solid line. The reflection coefficient of the numerical analysis increased as the wave period decreased. However, the resonance of the moored floating structure caused a large motion corresponding to the structure's natural period in each mode of motion, which enhanced the reflecting ability of the structure. The natural period of the structure decreased in range as the thin skirts changed their direction from vertical to horizontal. A narrow band around the natural

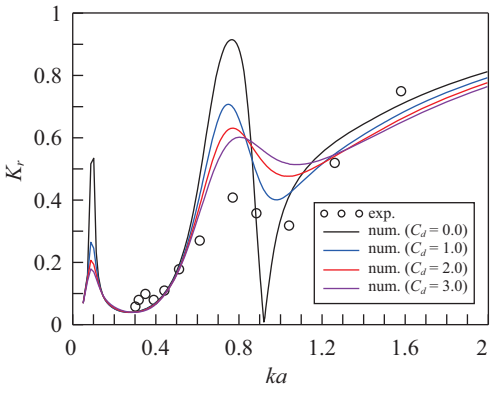

(a) α = 0°

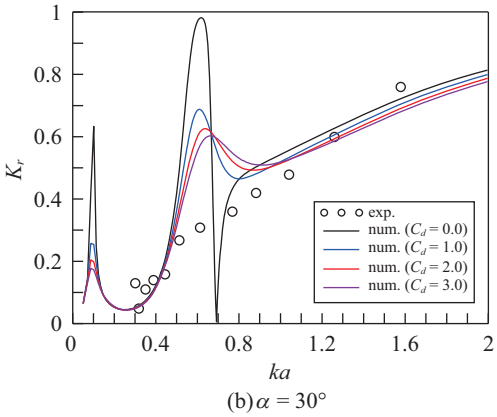

(b) α = 30°

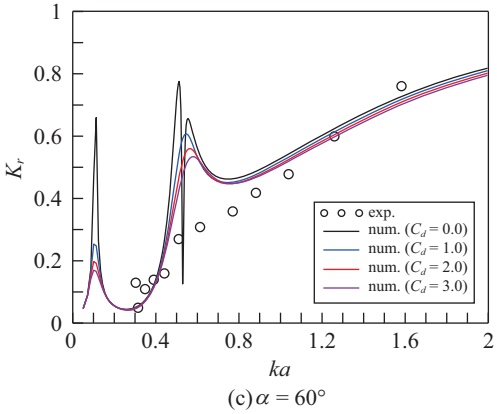

(c) α = 60°

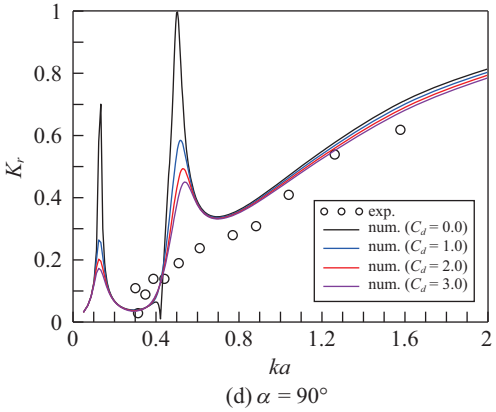

(d) α = 90°

Fig. 8. Correlation between reflection coefficient and ka for four angles of skirt (α = 0°, 30°, 60°, and 90°).

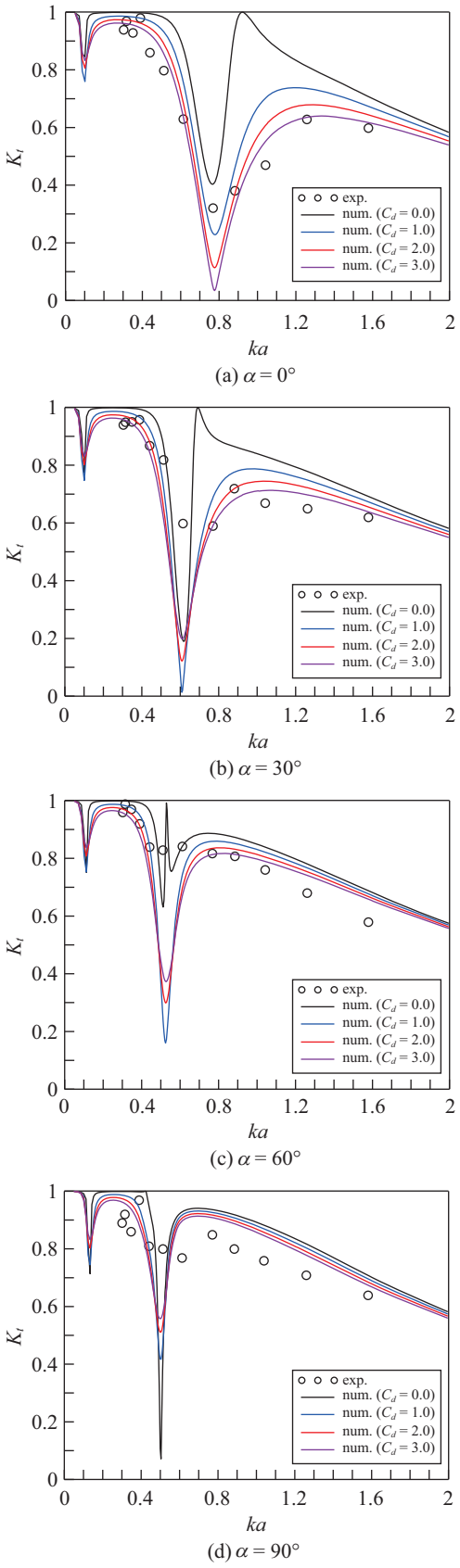

Fig. 9. Correlation between transmission coefficient and *ka* for four angles of skirt (α = 0°, 30°, 60°, and 90°).

period indicates a decreasing influence of the resonance period on the structure's motions and its reflecting ability, possibly because the reflection coefficients of the experiment scatter linearly when the skirt is at an oblique angle (α = 30°, 60°, and 90°).

The effect of the drag damping term on the reflection coefficient was similar to that in previous descriptions of structural motions, thereby providing an improved solution particularly as the natural period of the structure approached. As the figure illustrates, the analytical results around the natural period of the structure gradually decrease in value and approach the experimental results as the drag coefficient increases from 0.0 to 3.0. In contrast with the results of structural motions, there is still a significant difference between the analytical and experimental results near the natural period.

Figs. 9(a)~(d) shows the correlation between transmission coefficient and *ka* for four angles of skirt-attachment. As shown in Fig. 9(a), results of the test agree with those of the analysis when the drag coefficient is equal to 3.0, except near the natural period of structure (*ka* = 0.8). Thus, it indicates that increasing the drag term and a suitable drag coefficient are capable of enhancing the efficiency of analytical model, but there is still a significant difference between the experimental and numerical results near the natural period of the structure. The difference near the natural period of the structure increases as the angle of the skirt becomes horizontal.

The total energy in analytical Region (II) was discussed here for comprehending the effect of the nonlinear drag term on wave energy. According to the law of conservation of energy, energy in analytical Region (II) must be constant and can be expressed by the reflection and transmission coefficients, i.e. $E_T = K_r^2 + K_t^2 = 1$. However, some loss of energy occurs when vortex shedding appears or drags on the surface of structure because of the viscosity of the fluid. Figs. 10(a)~(d) show the distribution of total energy using analytically measured data. It was found that energy loss happens in all cases of experimental results. Besides, the area of major energy loss largely concentrates in the neighborhood of the natural period of the structure. This demonstrated that the resonance period of the structure is a critical factor affecting energy loss during the structure's movement. With the added drag term, numerical analysis provides a better solution and effectively describes the transformation of energy in the inner analytical domain.

VI. CONCLUSIONS

In this study, a numerical model was applied using the DBEM to analyze the dynamic behavior of a moored floating structure with two rigid skirts attached to the bottom. The thickness of the skirt was assumed to be zero. Nonlinear drag terms were also considered during the theoretical analysis. Discussions focused on the influences of the nonlinear drag term and the angle of skirt-attachment on structural motion, reflection, and transmission coefficients. The conclusions can be summarized as:

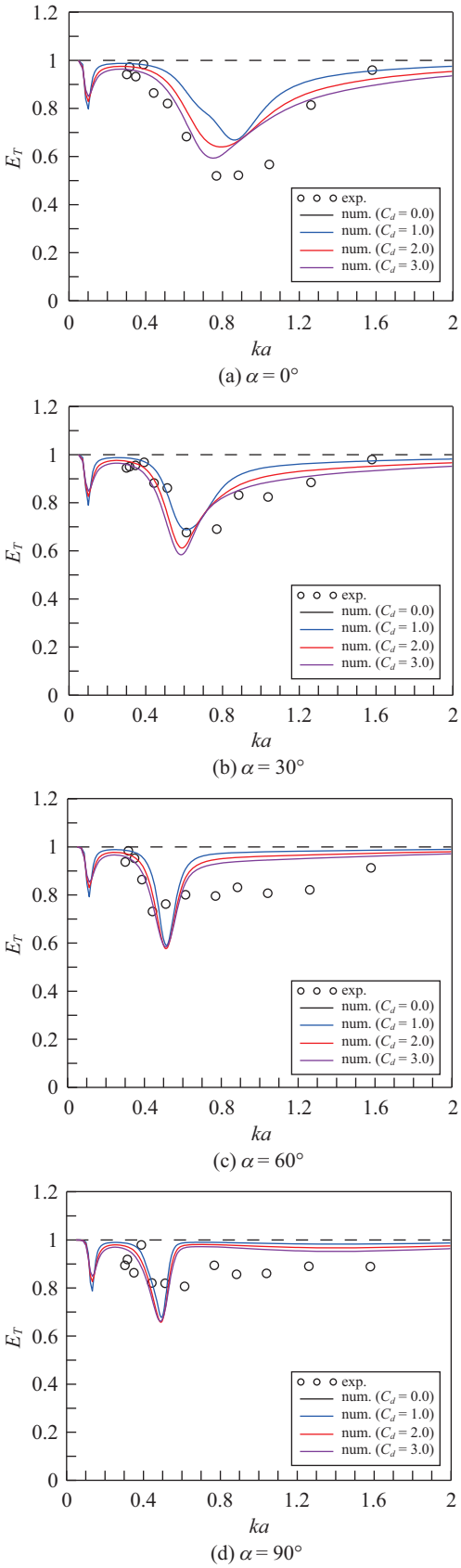

Fig. 10. Correlation between total energy and *ka* for four angles of skirt (α = 0°, 30°, 60°, and 90°).

1) The numerical model is capable of analyzing the motions of a moored floating structure with rigid and extremely thin skirts attached to the structure's bottom at different attaching angles, and its validity was verified by comparing the analytical results with experimental results.
2) The inclusion of a nonlinear drag term in the numerical analysis provides a better solution, with regard to structural motions and energy transformation, particularly as the natural period of the structural approaches.
3) The resonance period of a structure is a critical factor affecting energy loss during structural motions. The area of major energy loss is largely concentrated around the natural period of the structure.

REFERENCES

Chakrabarti, S. K. (1987). Hydrodynamics of Offshore Structures, Computational mechanics Publications, Boston.

Chen J. T. and H. K. Hong (1983). Boundary Element Method, New-World Taipei. (in Chinese)

Gesraha, M. R. (2006). Analysis of Π shaped floating breakwater in oblique waves: I. Impervious rigid wave boards. Applied Ocean Research 28, 327-338.

Goda, Y. and Y. Suzuki (1976). Estimation of incident and reflected waves in random wave experiments. Proceedings of 15th International Conference on Coastal engineering, Honolulu, Hawaii, Chapter 48, 828-845.

Huang, C.-C. and H.-J. Tang (2009). Dynamic Responses of Moored Floating Dual Pontoon Structure in a Fully Nonlinear Numerical Wave Tank. Proceedings of the Nineteenth International Offshore and Polar Engineering Conference, Osaka, Japan, 414-421.

Isaacson, M. and R. Byres (1988). Floating breakwater response to wave action. Proceedings of 21st Coastal Engineering Conference 3, 2189-2200.

Lee, J. and W. C. Cho (2003). Hydrodynamic analysis of wave interactions with a moored floating breakwater using the element-free Galerkin method. Canadian Journal of Civil Engineering 30(4), 720-733.

Lee, C.-P. and W.-K. Ker (2002). Coupling of linear waves and a hybrid porous TLP. Ocean Engineering 29(9), 1049-1066.

Lu, L., B. Teng, L. Sun and B. Chen (2011). Modelling of multi-bodies in close proximity under water waves-Fluid forces on floating bodies. Ocean Engineering 38(13), 1403-1416.

McCartney, B. L. (1985). Floating breakwater design. Journal of Waterway, Port, Coastal and Ocean Engineering, ASCE 111(2), 304-318.

Murali, K. and J. S. Mani (1997). Performance of cage floating breakwater. Journal of Waterway, Port, Coastal and Ocean Engineering, ASCE 123, 172-179.

Sannasiraj, S. A., V. Sundar and R. Sundarvadivelu (1998). Mooring forces and motion responses of pontoon-type floating breakwaters. Ocean Engineering 25(1), 27-48.

Sannasiraj, S. A., R. Sundarvadivelu and V. Sundar (2000). Diffraction-radiation of multiple floating structures in directional waves. Ocean Engineering 28(2), 201-234.

Wang, H. Y. and Z. C. Sun (2010). Experimental study on the influence of geometrical configuration of porous floating breakwater on performance. Journal of Marine Science and Technology 18(4), 574-579.

Weng, W. K. and C. R. Chou (2007). Analysis of response of floating dual pontoon structure. China Ocean Engineering 21(1), 91-104.

Williams, A. N. and W. G. McDougal (1996). A dynamic of submerged breakwater. Journal of waterway, Port, Coastal and Ocean Engineering 22(6), 288-296.